Structures of Apolipoprotein A-II and a Lipid−Surrogate Complex Provide Insights into Apolipoprotein−Lipid Interactions[†,‡]

M. Suresh Kumar,[§] M. Carson,[§] M. Mahmood Hussain,[||] and H. M. Krishna Murthy*[,§]

Center for Biophysical Sciences and Engineering, University of Alabama at Birmingham, 1530 3rd Avenue South, Birmingham, Alabama 35294, and Departments of Anatomy and Cell Biology and of Pediatrics, SUNY Downstate Medical Center, Brooklyn, New York 11210

Received May 3, 2002; Revised Manuscript Received July 29, 2002

ABSTRACT: Apolipoproteins A-I and A-II form the major protein constituents of high-density lipid particles (HDL), the concentration of which is inversely correlated with the frequency of heart disease in humans. Although the physiological role of apolipoprotein A-II is unclear, evidence for its involvement in free fatty acid metabolism in mice has recently been obtained. Currently, the best characterized activity of apolipoprotein A-II is its potent antagonism of the anti-atherogenic and anti-inflammatory activities of apolipoprotein A-I, probably due to its competition with the latter for lipid acyl side chains in HDL. Many interactions of apolipoprotein A-I with enzymes and proteins involved in reverse cholesterol transport and HDL maturation are mediated by lipid-bound protein. The structural bases of interaction with lipids are expected to be common to exchangeable apolipoproteins and attributable to amphipathic α-helices present in each of them. Thus, characterization of apolipoprotein−lipid interactions in any apolipoprotein is likely to provide information that is applicable to the entire class. We report structures of human apolipoprotein A-II and its complex with *β*-octyl glucoside, a widely used lipid surrogate. The former shows that disulfide-linked dimers of apolipoprotein A-II form amphipathic α-helices which aggregate into tetramers. Dramatic changes, observed in the presence of *β*-octyl glucoside, might provide clues to the structural basis for its antagonism of apolipoprotein A-I. Additionally, excursions of individual molecules of apolipoprotein A-II from a common helical architecture in both structures indicate that lipid-bound apolipoproteins are likely to have an ensemble of related conformations. These structures provide the first experimental paradigm for description of apolipoprotein−lipid interactions at the atomic level.

Exchangeable apolipoproteins are the protein constituents of high-density lipoproteins (HDL).[1] HDL are the mediators of reverse cholesterol transport (RCT), a process that removes excess cholesterol from cell membranes of peripheral tissues resulting in protection against arteriosclerosis (*1*−*5*). Enhancement of RCT is thought to possess significant potential for antiatherosclerotic drug therapy (*6*). Although several apolipoproteins are associated with HDL, apolipoproteins A-I (apo A-I) and A-II (apo A-II) account for most of their protein content in a 2:1 molar ratio (*7*). Apo A-I has a clearly defined role in human RCT, while that of apo A-II is unclear (*2*, *8*). Nevertheless, studies in genetically modified mice show a positive correlation between apo A-II and plasma free fatty acid and triglyceride levels, while its deficiency has been associated with increased atherosclerosis and insulin hypersensitivity (*9*). Apo A-II also counteracts several beneficial effects of apo A-I in humans, including diminishing the latter's atheroprotective and anti-inflammatory roles (*10*, *11*). The apo A-I antagonist ability of apo A-II might be a consequence of its higher affinity for lipids which permits it to displace apo A-I from HDL (*12*−*14*). Displacement of apo A-I from HDL affects the interaction of the particles with proteins involved in exchange of neutral lipid, lipolysis of triglycerides, and HDL remodeling (*12*, *15*, *16*).

Interactions of apolipoproteins with enzymes such as lecithin:cholesterol acyl transferase (LCAT) and receptors such as ATP-binding cassette transporter 1 (ABC1) and scavenger receptor class B type I (SR-BI) play an important role in RCT (*17*−*21*). An indispensable part is played by association of apolipoproteins with lipids in interactions of the former with enzymes and receptors involved in HDL remodeling. Lipid binding by apolipoproteins both enhances their helical content and helps in achieving appropriate relative juxtaposition of distant parts of the protein necessary for productive contact with enzymes and receptors (*16*, *20*, *22*). For example, LCAT interacts with HDL-bound apo A-I through several positively charged side chains of residues

[†] These studies were supported, in part, by NIH grants to M.M.H., who is also an Established Investigator of the American Heart Association.

[‡] Atomic coordinates for the structures described in this report have been deposited in the Protein Data Bank as entries 1L6K (free-A-II) and 1L6L (A-II-BOG).

* To whom correspondence should be addressed: CBSE 100, 1530 3rd Ave. South, Birmingham, AL 35294-4400. Phone: (205) 934-9148. Fax: (205) 934-0480. E-mail: murthy@io.cbse.uab.edu.

[§] University of Alabama at Birmingham.

[||] SUNY Downstate Medical Center.

[1] Abbreviations: apo A-I and A-II, apolipoproteins A-I and A-II, respectively; HDL, high-density lipoproteins; RCT, reverse cholesterol transport; BOG, *β*-octyl glucoside; free-A-II, structure of apo A-II in the absence of added detergent; POPC, 1-palmitoyl-2-oleoyl-*sn*-glycero-3-phosphocholine; A-II-BOG, structure of apo A-II in the presence of submicellar concentrations of BOG; A-II-micellar, structure of apo A-II in the presence of micellar concentrations of BOG.

10.1021/bi026069w CCC: $22.00
Published on Web 09/07/2002

between positions 144 and 186 of the latter (*23*). The two helices that that make up this region of apo A-I in its lipid-bound conformation (*24*), helix 6 (residues 145−174) and helix 7 (residues 175−186), position three Arg residues (positions 151, 160, and 173) appropriately for interaction with negatively charged residues on LCAT (*25*). Interactions of all exchangeable apolipoproteins with lipid in HDL are expected to be mediated by 11-residue amphipathic helices (*26*−*29*) which position hydrophobic side chains to generate surface patches that associate with acyl side chains of lipids. Indeed, structures of apolipoprotein fragments in the absence of lipid have revealed such helices (*24*, *30*−*32*). However, no experimental structures of apolipoprotein−lipid complexes exist; although the structure of apo C-II has been determined in the presence of the detergent sodium dodecyl sulfate (*33*), its convex hydrophobic face inexplicably contradicts all current experimental observations. Thus, descriptions of the interaction between apolipoproteins and lipids, in the absence of suitable experimentally determined structures, have relied on a variety of indirect computational, biophysical, biochemical, and mutagenesis studies (*26*−*28*). Because of the central role that lipid−protein interactions play in RCT, and the postulated role for enhancement of RCT in atherosclerosis therapy (*6*), directly visualizing these interactions in any lipoprotein is of immense interest. The anticipated universality of the mode of interaction between exchangeable apolipoproteins and lipid acyl chains makes delineation of interaction details in any one apolipoprotein an informative model for the entire class.

We present crystal structures of human apo A-II in a lipid-free environment (free-A-II) and in the presence of submicellar concentrations of β-octyl glucoside (BOG, A-II-BOG), a detergent that is widely used in membrane protein solubilization and crystallization as a structural and functional lipid surrogate (*34*). Together, these structures demonstrate structural plasticity and the specific self-association property of apo A-II which might be relevant to its interaction with lipids. The A-II-BOG structure provides the only experimental paradigm, at this time, for structural descriptions of apolipoprotein−lipid interactions.

EXPERIMENTAL PROCEDURES

Crystallization and Data Measurement. Purified apo A-II, isolated from human HDL (*35*), was obtained from the core laboratory of the Department of Biochemistry, Medical College of Pennsylvania (Philadelphia, PA). All three crystal forms were obtained from solutions containing 12.5−20 mg/mL (1.2−2.3 mM) apo A-II using hanging drop setups. Wells for growing free-A-II crystals contained 200 mM cacodylate buffered to pH 5.6−6.2, 2 mM $CoCl_2$, 2 mM $NiCl_2$, 0.5 mM cobalt hexamine chloride, 40 mM LiCl, and 30−45% MPD; drops were made up by mixing equal volumes of well solutions with the protein solution. The BOG-bound form of apo A-II (A-II-BOG) was crystallized in the presence of ~19 mM (0.65%) BOG, in addition to components used for free-A-II. The critical micellar concentration (CMC) for BOG is ~22−24 mM (*34*); thus, the BOG concentration in A-II-BOG, assuming a 2-fold increase in the concentration of components in the drop, is ~73% of the CMC. Diffraction data for both crystal forms were measured on flash-frozen crystals after transferring them to 65−75% MPD. Measurements were taken on a Siemens X1000 multi-wire area detector system (Rigaku RU200, $\lambda = 1.5418$ Å), and the data were processed using XDS (*36*). Crystallographic parameters and data processing statistics are given in Table 1.

Table 1: Measurement and Processing of Data for Sm Derivatives[a]

	free-A-II	A-II-BOG
cell dimensions		
distances (Å)	93.7, 126.4, 102.9	114.4, 115.9, 126.6
angles (deg)	90.0, 90.7, 90.0	90.7, 96.2, 93.5
space group	$P2_1$	$P1$
resolution (Å)	30 (2.7−2.5)	30 (2.7−2.6)
completeness [% > $2\sigma(I)$]	90 (88)	87 (61)
R_{sym}[b]	0.066 (0.109)	0.052 (0.081)
R_{bij}[c]	0.172 (0.266)	0.133 (0.178)
R_{cen}[d]	0.057 (0.118)	

[a] Values in parentheses correspond to the highest-resolution shell. [b] $\sum|I - \langle I\rangle|/\sum I$, for all symmetry mates, except in the case of A-II-BOG where the summation is over multiple observations. [c] $\sum|F^+ - F^-|/\sum F^+ + F^-$, for Bijvoet mates. [d] Same as 2 for *hol* reflections only.

Table 2: Structure Solution and Refinement[a]

	free-A-II	A-II-BOG
phasing		
F_{om}[b]	0.67 (0.61)	0.66 (0.58)
PhP[b]	2.62 (2.11)	2.60 (2.20)
F_{om}[c] (Dm)	0.76 (0.74)	0.75 (0.71)
refinement		
resolution (Å)	8 (2.1−2.0)	8 (2.4−2.3)
R_{sym}	0.045 (0.078)	0.059 (0.099)
completeness [% > $2\sigma(I)$]	93 (74)	88 (79)
$\langle I/\sigma(I)\rangle$	15.9 (10.4)	10.3 (5.1)
redundancy	4.0 (2.1)	2.3 (1.9)
R_{cryst}	0.187 (0.220)	0.198 (0.247)
R_{free}[d]	0.219 (0.266)	0.238 (0.289)
rmsd for bonds (Å)	0.01	0.01
rmsd for angles (deg)	1.1	1.0
$\langle B\rangle$ (protein, water, BOG)	27.9, 44.2, −	29.2, 54.8, 39.9

[a] Values in parentheses correspond to the highest-resolution shell. [b] Figure of merit and phasing power defined in ref *49*. [c] Figure of merit defined in ref *39*. [d] For 10% of the reflections chosen randomly to span the resolution range.

Structure Solution and Refinement. Both free-A-II and A-II-BOG structures were determined using a single heavy atom derivative each, obtained by soaking crystals in buffers containing 5 mM $SmCl_3$ in addition to components used for crystallization. Single isomorphous replacement supplemented with the use of anomalous scattering (SIRAS) differences provided a starting phase set. Initial solutions from SOLVE (*37*) were refined with MLPHARE (*38*). Nine major and three minor sites were detected for free-A-II and 31 major sites and five minor site for A-II-BOG. Phases were refined by solvent flattening and NCS averaging (3-fold among tetramers in free-A-II and 2-fold among 16 chain arrays in A-II-BOG) using Dm (*39*). Figures of merit and other SIRAS phasing statistics are given in Table 2. Atomic models for A-II and BOG were built into Dm (*39*) maps with O (*40*). Both structures were refined with CNS (*41*) using Engh−Huber (*42*) parameters for geometric restraints. Noncrystallographic symmetry restraints, for protein but not BOG residues, were employed in addition to geometric restraint,; among trimers in free-A-II and the two arrays in A-II-BOG. Tight restraints on coordinates in initial stages were relaxed in the final stages. *B* factors were tightly restrained throughout. Data between 8 and 2.0 Å for free-

Table 3: Model Composition and Quality

	free-A-II	A-II-BOG
no. of protein residues (in model/total)	869/924	2366/2464
no. of BOG residues	0	67
no. of water oxygens	761	1522
total no. of non-hydrogen atoms	7666	21619
no. of Ramachandran outliers	0	6[a]

[a] There is strong unambiguous density for placing these residues in their current positions.

A-II and 8 and 2.3 Å for A-II-BOG in which $F > 2\sigma$ were included in refinement. R_{free}s helped monitor the refinement using 10% of the reflections chosen randomly to span the resolution range. A search for water molecules was made, and their positions and *B* factors were refined for several cycles, retaining those that refined to reasonable *B* factors and hydrogen bonding geometry as part of the final model. *R* values and other refinement statistics are shown in Table 2 and the model composition and quality parameters in Table 3. An attempt was made to search for metal ions in both structures since Co- and Ni-containing compounds were used as additives in crystallization. However, no Co^{2+} or Ni^{2+} ions could be located in either free-A-II or A-II-BOG structures by analysis of difference Fourier or Bijvoet difference maps phased with refined models. The latter were computed from data, measured at 1.5418 Å for Co^{2+} and 1.4864 Å (NSLS/X4A) for Ni^{2+}, on native crystals; both wavelengths are on the high-energy side of the respective K absorption edges. All figures have been prepared with RIBBONS (*43*). Wavelet approximations to helical paths in Figures 2a, 3a, and 6 were calculated according to the method of Carson (*43*). An all-atom model of a discoidal complex consisting of 20 molecules of 1-palmitoyl-2-oleoyl-*sn*-glycero-3-phosphocholine (POPC) simulated through molecular dynamics within a solvated sphere (*44*) was used to make Figure 6b. The surface in Figure 6b was computed using an algorithm by Connolly (*45*) and a probe radius of 1.4 Å. All solvent accessibility calculations were performed using AREAIMOL with a 1.4 Å probe in CCP4 (*46*).

RESULTS

Structure of Lipid-Free Apo A-II (Free-A-II). Two representative sections of electron density maps, depicting the experimental density for identical parts of the protein in free-A-II (a) and A-II-BOG (b), are shown in Figure 1. Human apo A-II is a homodimer of 77 residue chains linked through a single disulfide bond, although it also exists as a heterodimer with apo E and apo D. It is synthesized as a pre-proprotein, is proteolytically processed into its mature form, and mainly remains associated with HDL in human plasma (*47*, *48*). The asymmetric unit of free-A-II has a hierarchical organization (Figure 2a) with a disulfide-bonded dimer forming the basic unit (Figure 2b). Two dimers associate to form a tetramer, held together mostly by complementary interactions between their hydrophobic patches (Figure 2c). Three tetramers associate into a dodecamer related by approximate 3-fold noncrystallographic symmetry to complete the asymmetric unit. Fifty-five of the 924 residues in the dodecamer are not seen in electron density maps, including the three N-terminal residues and the C-terminal Gln in each chain and residues 6−9 in some chains. Three long α helices (H1−H3) make up most of the structure of each monomer (Figures 2 and 3a). The limits of helices vary somewhat among A-II molecules (Figure 3a) that form the parallel helical bundle, with some of the helices having significant bends (Figure 2a). Helices are largely punctuated at prolines, although not uniformly so (Figure 3a), unlike in the structure of apo A-I (*24*). Short (three- or four-residue) 3_{10} helices occur in many chains between α helices (Figure 3a). The interhelical residues largely display conformational angles typical of the type IV β turn, although some have angles closer to that of type I turns (*49*). The monomer interactions in the dimer are not extensive (Figure 2b), with each chain losing ∼14% of its solvent accessible surface and making 11 hydrogen bonds on average. Three hydrophobic patches are clearly distinguishable in each dimer, comprising residues 6−29, 41−53, and 60−70 (Figures 2b and 3a) from each chain. Although the terminal patches are nearly continuous, an aromatic cluster including Tyr41 and Phe42 spatially separated from an aliphatic clump composed of Leu52 and Ile53 makes up the middle patch. The two dimers in a tetramer interact much more extensively (Figure 2c) through corresponding hydrophobic patches with each dimer losing an average of 30% of its solvent accessible surface to tetramerization. There are also on average 25 hydrogen bonds between dimers. Interactions between tetramers are relatively few and mostly hydrophilic.

Structure of Apo A-II Complexed with β-Octyl Glucoside (A-II-BOG). Two copies of 16 apo A-II dimers, arranged in an irregular double-stranded helical array (Figure 4a) form the asymmetric unit of the structure. The hexadecameric arrays are related by an approximate 2_1 screw (167° rotation, 0.503**a** translation), nearly along the **a** axis, with an rms deviation for 1158 common Cα atoms of 1.9 Å. The only residue without visible electron density in all chains is the amino-terminal Gln, making it the only residue systematically absent in both structures; every other residue is represented in 10 or more chains. Examination of electron density maps showed residual density at the expected locations of the N-terminal Gln residue in several chains; however, the density was not consistent enough to model this residue. Each strand of the hexadecameric array (Figure 4a) consists of an octamer of apo A-II chains, built from a noncovalently linked, head-to-tail assembly of disulfide-linked dimers. In the inner strand (chains A−H), helix H1 is nearly unchanged, compared to that in free-A-II, while H2 and H3 are more frequently interrupted by β bends (Figure 3a,b). The outer strand (I−Q) helices are, in contrast, more fragmentary, being in many cases shorter than those in free-A-II (Figure 3a,b). Several helices also show significant bends (Figure 4a). The helices in both strands are generally, although not invariably, punctuated at prolines (Figure 3b). The orientation of helices again places hydrophobic patches on the same side of the dimer planes (Figure 4b). The monomers interact with each other even less than in free-A-II, with an average of seven hydrogen bonds and a loss of ∼10% of solvent accessible surface on dimerization; in part, the more tenuous interaction is due to the presence of an average of eight BOG molecules at each tetramer interface. This interface is mostly composed of hydrophobic side chain interactions, with an average of 155 van der Waals (vdW) contacts per chain among protein side chains, in three patches, as in free-A-II (Figure 2b). There are few electrostatic interactions; the A−I interface,

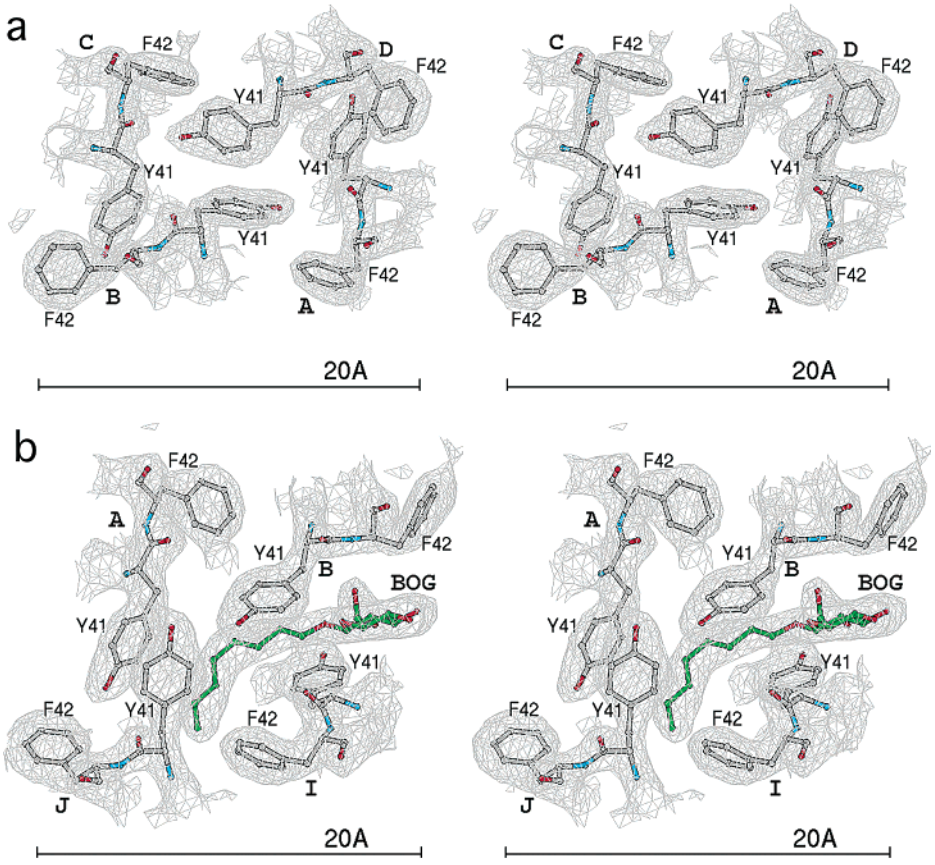

FIGURE 1: Experimental electron density. The $2F_o - F_c$ maps, phased by the final model, contoured at 1.7σ are shown, with the final model superimposed. Carbons are colored gray, nitrogens cyan, and oxygens red. (a) Residues Tyr41 and Phe42 in chains A−D in free-A-II. (b) The same residues in A-II-BOG along with the BOG residue that contacts these apo A-II residues, shown with carbons in green and oxygens in red.

for example, has no electrostatic interactions, while the E−M interface has the maximum of eight electrostatic interactions. Neither the free-A-II nor the A-II-BOG structure is similar to the atomic model proposed for apo A-II (*50*), based on uteroglobin.

In both the free-A-II and A-II-BOG structures, the arrangement of helices most closely resembles that observed in the apo A-I structure (*24*), although the former is made up of shorter helices. Lengths of helices are also shorter in the two apo A-II structures than in the apo E fragment (*31*) and apolipophorin structures (*30*, *32*). Packing of helices in both apo A-II structures is also quite different from that seen in the apo E and two lipophorin structures. In free-A-II, the helices pack in a nearly straight side-by-side tetrameric array (Figure 2a), while in A-II-BOG, the helices adopt a variety of curvatures, although they still remain tetrameric (Figure 4a). Both apo E and apolipophorin structures, on the other hand, are composed of classic antiparallel four-helix bundles constructed from covalently linked helices.

BOG Molecules in A-II-BOG. We have located a total of 67 BOG molecules in apo A-II-BOG, which are strategically spaced to interact with A-II hydrophobic patches (Figures 3b and 4a,b). There are 31 complete and three partial molecules in array 1 and 32 complete and one partial molecules in array 2. The 31 molecules common to the two arrays occupy nearly identical positions, with respect to the protein, and have closely similar conformations in the two arrays, with an rms deviation of 1.5 Å for 620 common atoms. The octyl side chains are largely orthogonal to the local protein helical axes (Figure 4b) and make an average of 43 vdW contacts each, predominantly with hydrophobic protein side chain atoms. Each octyl side chain loses ~84% of its solvent accessible surface area of 289 Å^2 on complex formation, which is roughly equal to the area of the inner and outer strands of the arrays. Each protein chain in the octamer loses, on average, 10% of its solvent accessible area to BOG interactions and approximately 20% to protein−protein interactions. The glucosyl ring oxygens of BOG molecules in A-II-BOG form several hydrogen bonds, primarily with main chain O and N atoms, since these are the only polar atoms in the strongly hydrophobic environments of the side chains. Each glucosyl headgroup makes, on average, 38 vdW interactions with apo A-II atoms and one hydrogen bond; 26 of the 37 hydrogen bonds in each array are with main chain O or N atoms.

DISCUSSION

Dimerization and Helicity in Apo A-II. Disulfide-mediated dimerization is not essential for lipid association by apo A-II, as its activity is impaired little on reduction and carboxymethylation (*14*). The accessible surface areas buried in dimer formation in free-A-II (14%) and A-II-BOG (10%) are both lower than average (17%) for a small (<100 residues) protein (*51*); considered along with the sparseness of other monomer interactions, this corroborates the adventitious rather than functionally mandated nature of apo A-II dimerization (*14*). Oligomerization of apo A-II, beyond a

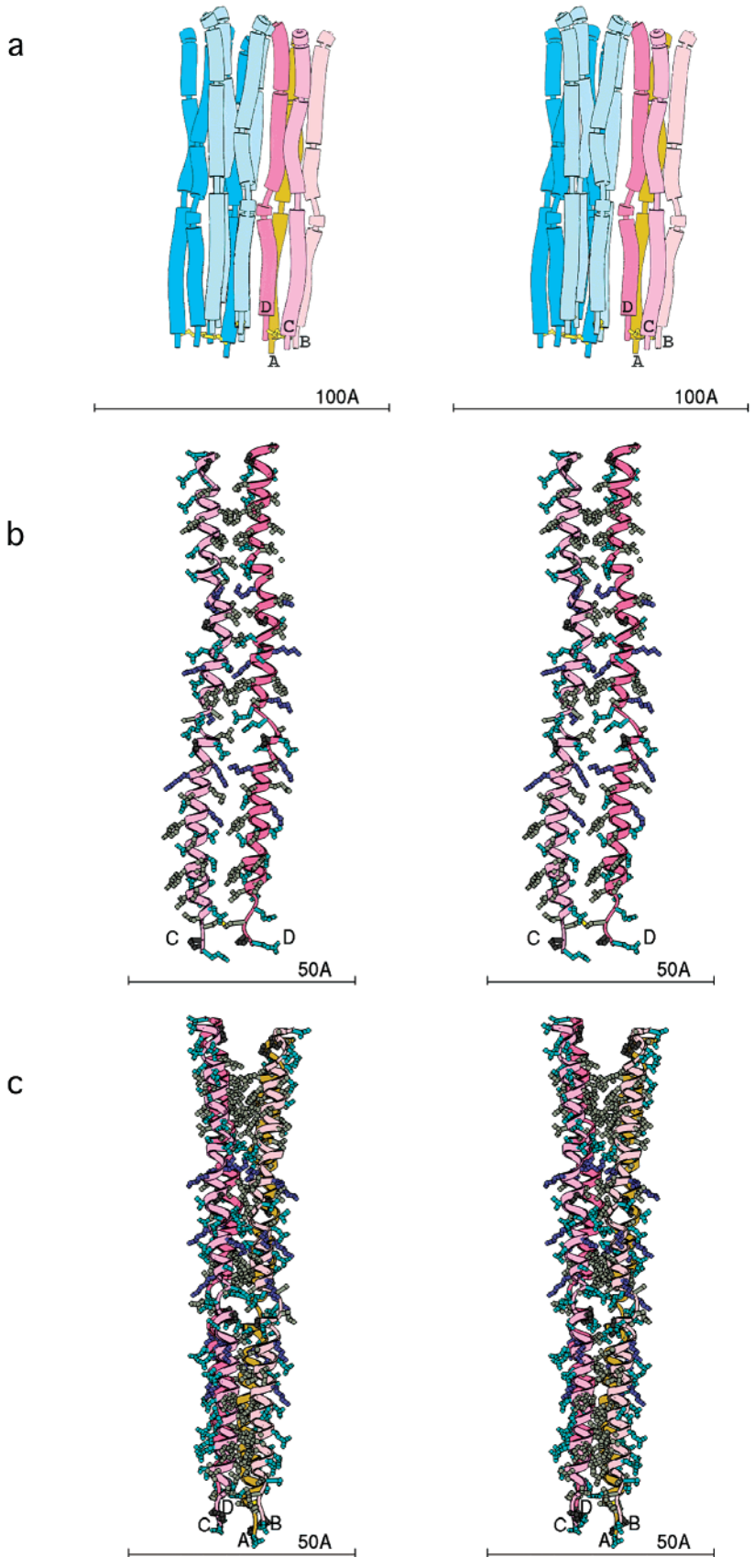

FIGURE 2: Lipid-free apolipoprotein A-II. (a) A stereopair of the 12 independent chains is shown as wavelet approximations to chain paths with helical residues shown as thick tubes. The four chains of the first tetramer (A−D) are given different colors, and the other two tetramers are colored shades of blue. Yellow bonds designate the disulfide linkages. (b) The disulfide-linked homodimer has each backbone represented by a ribbon, colored as in Figure 1a. The side chain atoms are colored by residue, with hydrophobic residues gray, polar residues cyan, and positively charged residues blue. The view is toward the hydrophobic face. (c) The tight association of two dimers to form the tetramer observed in the crystal packing. The coloring is as in Figure 1a. This view is perpendicular to that in panel b.

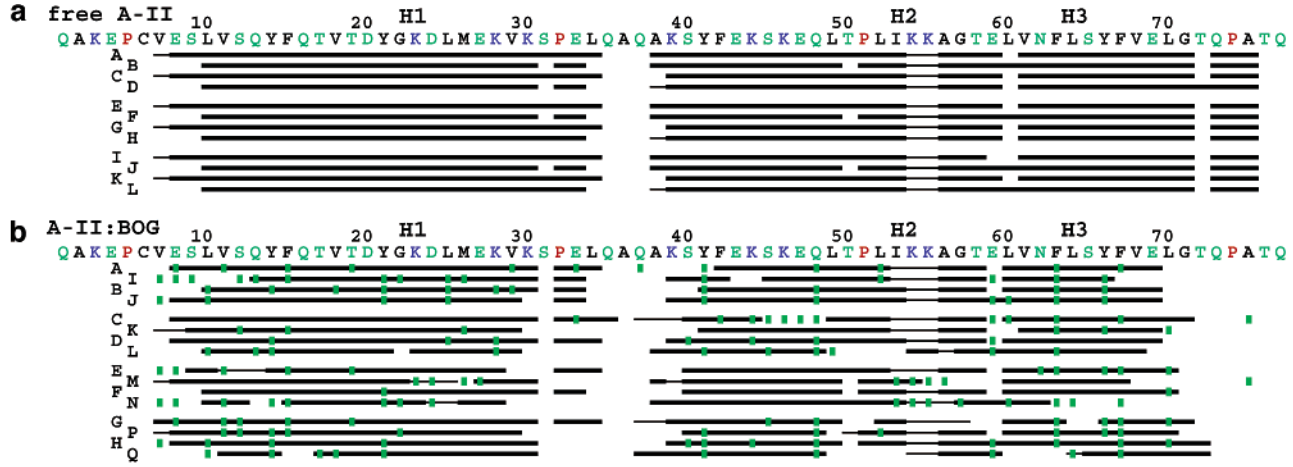

FIGURE 3: Sequence and secondary structure. The sequence of apolipoprotein A-II is shown with hydrophobic residues colored black, positively charged residues blue, polar residues cyan, and prolines red. The secondary structure of the individual chains is shown with thick lines for α helices and thin lines for 3_{10} helices. The secondary structure was determined from Cα positions only using a method implemented in Ribbons. Larger spacings separate groups of tetramers. Approximate midpoints of helices H1−H3 are marked. (a) The 12 independent chains of the lipid-free form are shown and labeled A−L. (b) The 16 independent chains of the BOG complex form are shown below, with the eight inner chains labeled A−H and the eight outer chains labeled I−Q, with the letter O not being used. Note that the chains are grouped into pairs of dimers that contact common BOG molecules. Small green rectangles indicate residues in apo A-II with which BOG molecules make contact.

dimer, has not been reported. However, the dimer has been shown to be of marginal stability (*52*), and studies on synthetic mimetics have implied formation of larger aggregates (*53*). The presence of higher-order oligomers in free-A-II could be due to the higher protein concentration in crystals that are normally not attained in other experimental systems. Nevertheless, multiple copies of apo A-II dimers are clearly associated with both HDL and synthetic phospholipid vesicles (*14*), indicating that oligomerization in A-II-BOG might be relevant to its organization in HDL. The helical content of most apolipoproteins increases upon association with lipid. For example, the percentage of α helix in apo A-II increases from a low of 30% in dilute solutions to 53−72% in the presence of lipid (*16*). Molecules in the free-A-II structure have helical contents between 77 and 83%; those in the inner strand of A-II-BOG range from 66 to 74%, and those in the outer strand range from 58 to 74%. Both free-A-II and A-II-BOG structures can be considered "lipid-associated" in the sense that each apo A-II dimer in free-A-II provides a complementary hydrophobic surface for the other in the tetramer (Figure 2b,c); helical contents in both are thus expected to be above the baseline value of 30%, as observed. However, the increase in helical content in both appears to be driven primarily through protein−protein interactions with the BOG residues in A-II-BOG having a comparatively minor effect, presumably due to the relative paucity of BOG molecules in the interface.

Head-to-Tail Association of Dimers in A-II-BOG. Comparison of free-A-II (Figure 2a) and A-II-BOG (Figure 4a) structures shows striking changes in the organization of apo A-II tetramers in the presence of BOG. Side-by-side packing of tetramers seen in free-A-II is replaced by sequential head-to-tail oligomerization of tetramers into an irregular double-stranded array in A-II-BOG. Five specific interactions form the foundation for stabilizing the head-to-tail association of dimers in A-II-BOG. Each of the two carboxylate oxygens of Gln77 forms hydrogen bonds with both the peptide nitrogen of Ala2 and an additional polar interaction with Nζ of Lys3 in the succeeding chain; in addition, Oε1 of Gln77 makes a polar interaction with Nζ of Lys3 in the succeeding chain (Figure 5a). These interactions are systematically present in both arrays, with 112 of 120 possible occurrences actually being observed.

In A-II-BOG, helix H2 is sharply inclined (Figure 5b), with respect to H1, with average interhelical angles of 122° for the inner strand (chains A−H) and 227° for the outer strand (chains I−Q). This plasticity permits apo A-II, in the presence of BOG, to adopt a spectrum of conformations with curvatures that fall on either side of the straight form observed in free-A-II (Figure 5b). The suppleness is the result of main chain flexibility in the region of residues 31−39 between helix H1 and H2. In the free-A-II structure, the dominant conformational motif in this region is the type IV β turn, although several type I turns also exist and residues 32−34 in several chains form a 3_{10} helix (Figure 3a). In A-II-BOG, residues 33−39 in most cases adopt no defined secondary structure (Figure 3b). As judged by rms deviations of Cα atoms from a common "average" structure (*54*), residues 31−39 in free-A-II are more similar (1.1 Å) than those in A-II-BOG (3.2 Å). Conformations of residues 31−39 are stabilized, in both structures, by mainly vdW contacts. In addition, hydrophilic side chains of Ser31, Gln33, Gln35, Gln37, and Lys39 form hydrogen bonds mostly with main chain atoms of the same chain.

The two octameric strands in each array are stabilized by complementary interactions between respective hydrophobic patches and BOG-mediated contacts. Most of the hydrophobic side chains occupy the convex side for the inner strand of the helical array, and concave side for the outer strand. Both spherical and discoidal HDL particles present convex binding surfaces to apolipoproteins. The latter form of the curved A-II-BOG array thus presents a surface that is complementary to that of HDL surfaces. Interestingly, the inner and outer octamers differ significantly in the extent of interaction between successive chains. The inner strand chains, as expected from the smaller radius of curvature, interact more extensively; D−F interactions, for example, occur through the range of residues 68−77 for chain D and

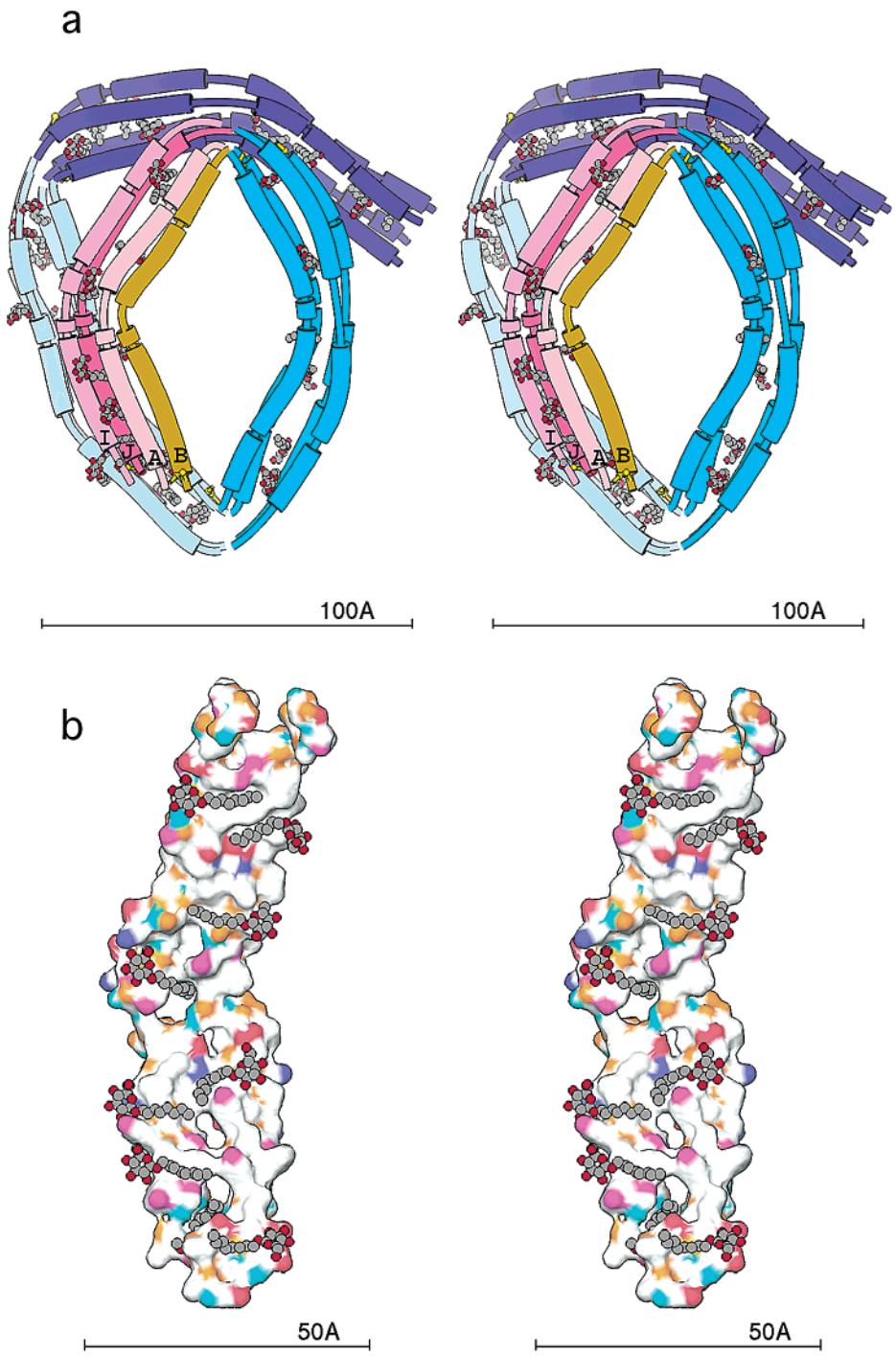

FIGURE 4: BOG-bound apolipoprotein A-II. (a) A stereopair of the eight independent dimers, of one of the two arrays in the asymmetric unit, is shown as wavelet approximations to chains as in Figure 1a. The four chains of the first tetramer (A, B, I, and J) are given different colors, and the other three tetramers are colored shades of blue. Yellow bonds designate the disulfide linkages. (b) The disulfide-linked homodimer (I−J), shown as a stereopair, is rendered as a surface colored by atomic property: white for hydrophobic atoms, blue for positive charges, cyan for H-bond donors, red for negative charges, orange for H-bond acceptors, and magenta for polar residues. The bound BOG molecules are shown as spheres with carbons gray and oxygens red. The amino termini of the chains are at the bottom.

residues 2−7 for chain F, mostly through vdW contacts, although there are several additional hydrogen bonds. However, the only systematically recurring specific interactions are the five enumerated above and shown in Figure 5a. In the outer strand, there are several additional vdW contacts, but these are limited to residue 77 in one strand with residues 2−4 in the succeeding strand. The residues involved in the head-to-tail interactions (Ala2, Lys3, and Gln77) are disordered in all chains of free-A-II; electron density for Ala2 and Lys3 is also absent for the N-terminal chains (A, B, I, and J) and for Gln77 in C-terminal chains (G, H, P, and Q) in each octamer of A-II-BOG in both arrays. The interchain association of apo A-II thus appears to be stable only when combined with BOG binding. The two hexadecameric arrays in A-II-BOG as well as the tetramers in apo A-II probably associate to shield hydrophobic residues for solvent contact. Similar association has been observed for apo A-I (*24*). Apo E (*31*) and apolipophorin III (*30*, *32*), on the other hand, form monomolecular helical bundles to achieve solvent shielding.

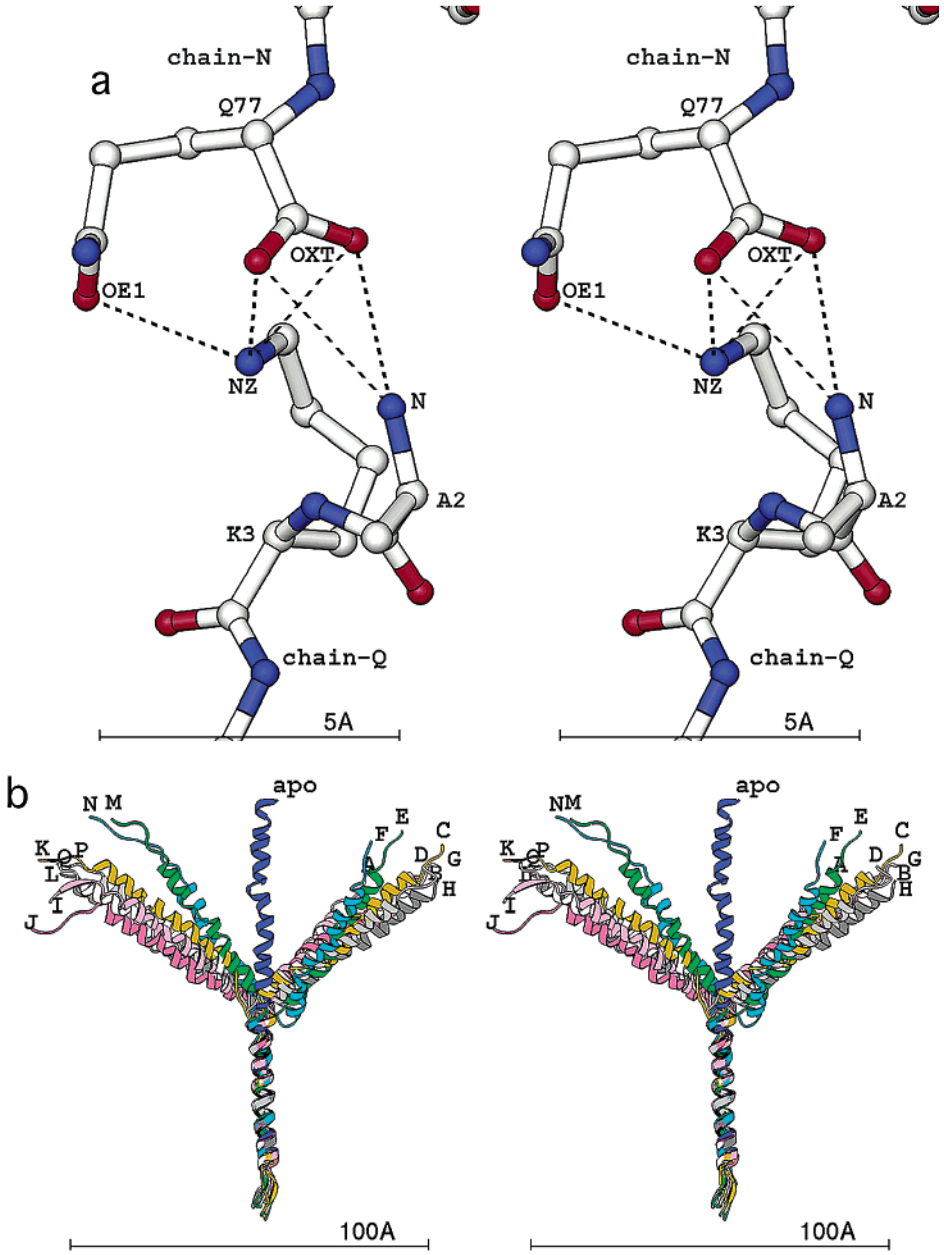

FIGURE 5: Head-to-tail association and chain flexibility. (a) A representative linkage between two outer chains (M and Q) is shown in detail, with possible hydrogen bonds marked with dashed lines. (b) The A chain of the lipid-free form (free-A-II, deep blue ribbon) is used as the reference. The 16 independent chains of the BOG complex are superimposed by a least-squares fit of the Cα atoms of residues 10−30. The ribbons are assigned eight arbitrary colors with each inner/outer pair colored the same.

Lipid-Driven Conformational Changes in Apolipoproteins. The salient observations that we make about the structures of apo A-II, the differences between the free and BOG-bound forms, the ability of apo A-II dimers to adopt different curvatures, the specific head-to-tail oligomerization, and the orientation of the octyl side chains of BOG to local helical axes of the protein all might have direct relevance to current models of apolipoprotein−lipid interactions. It is believed that conformations of apolipoproteins in their lipid-free or lipid-poor states differ significantly from those in their lipid-bound states (*27*, *28*). For example, in the lipid-free structure of apolipophorin III, the chain folds into a helical bundle with hydrophobic residues in the core (*30*, *32*); the structure of (Δ1−43)apo A-I, although in a lipid-free environment, is thought to be resemble the lipid-bound form of that protein (*24*, *27*). Large structural transitions, triggered by lipid binding, have been postulated to occur that convert lipid-free apolipophorin III to its lipid-bound configuration (*28*, *30*, *32*). Other apolipoproteins such as apo E also undergo such a conformational transition (*55*). The differences between the nearly straight rod conformation of free apo A-II and the curved octamers in apo A-II-BOG that we observe provide a dramatic experimental illustration of the magnitude of such lipid-driven changes. It is also evident that individual apo A-II dimers in both free and BOG-associated states do not have identical conformations. The variability that we observe provides experimentally derived parameters for adaptability of apolipoprotein conformation to the environment, which could be useful in modeling their interactions with lipids.

Apo A-II Flexibility and Lipid Binding. Recent models (*56*) of apo A-I binding to lipid disks have proposed interaction of a dimer with the lipid; earlier stoichiometric studies (*13*, *14*) have identified replacement of one molecule of apo A-I

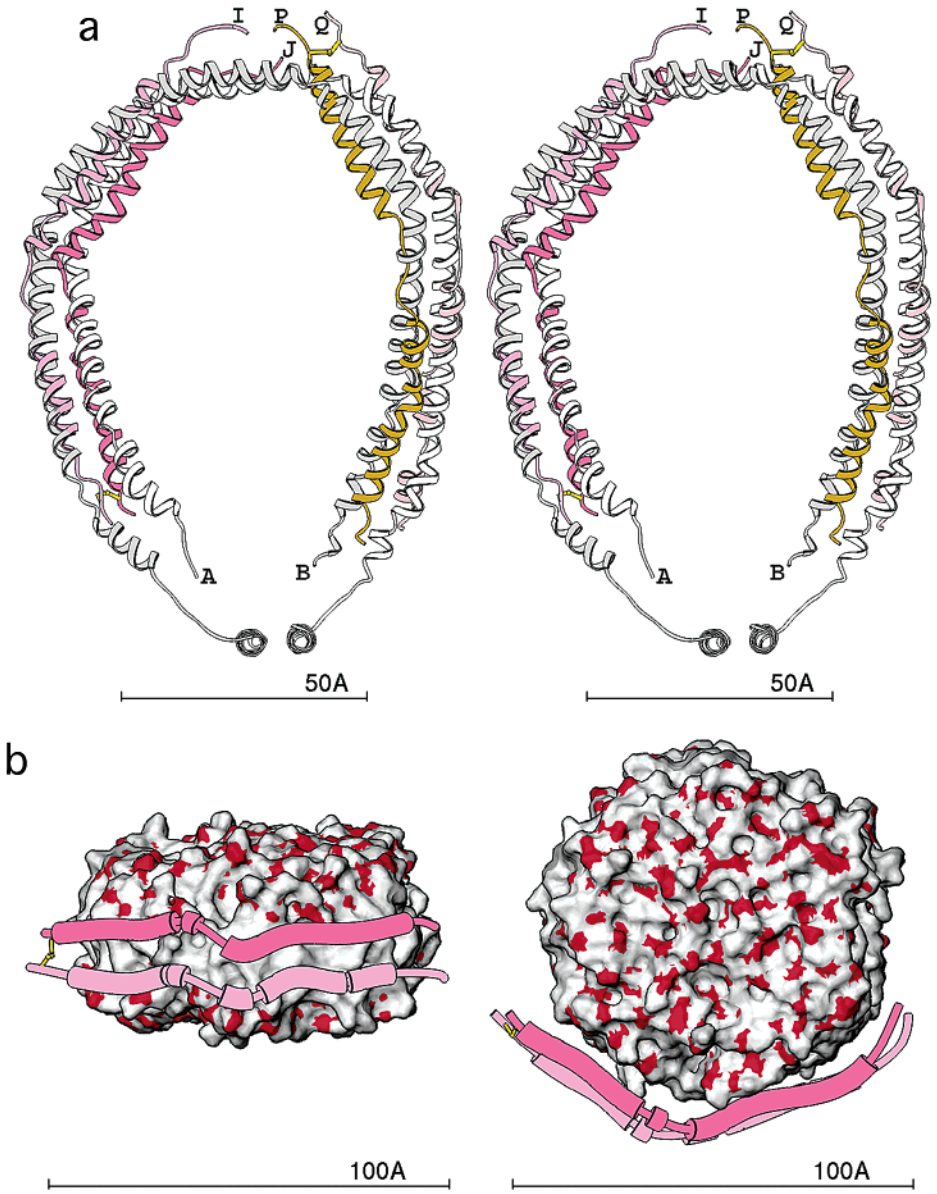

FIGURE 6: Model for lipid binding. (a) Superposition of the I−J and P−Q outer dimers in the BOG complex over the A−B dimer observed in the crystal structure of apolipoprotein A-I, shown as a stereopair. Each chain is shown as a differently colored ribbon, with the disulfides in the A-II structure shown as yellow bonds. The discoidal lipid bilayer model has been constructed using the molecular dynamics-derived coordinates of 20 POPC molecules solvated within a water sphere and reported in ref *44*. (b) The I−J dimer is wrapped around the lipid bilayer obtained from a model A-I−lipid disk structure, shown in two orthogonal views. The two chains are shown in wavelet representations as in Figures 1a and 3a. The bilayer surface is colored gray for carbons and red for phosphates.

with two molecules of apo A-II. The curvature seen in the apo A-I structure (*24*) can be mimicked by apo A-II dimers; using the I−J pair, a reasonable fit (rms deviation of 2.2 Å for 140 Cα pairs) can be achieved (Figure 6a) with the apo A-I A−B dimer. Superposition (Figure 6b) of the I−J dimer from A-II-BOG on the apo A-I molecular belt around a theoretical discoidal HDL model (*44*) also emphasizes the complementarity of A-II-BOG dimer curvatures to those of HDL particles. These observations on A-II-BOG also strengthen inferences about the conformation of apo A-I in its crystal structure (*24*) being that of the lipid-bound form. Circumferences of HDL particles vary from ∼155 Å for HDL_3 to ∼410 Å for HDL_2 with several intermediate values (*12*). It is thus important for an apolipoprotein to possess malleability that enables it to bind to particles with different curvatures. The flexibility at residues 31−39 in apo A-II makes possible an almost continuous adjustment of length and curvature as well as, potentially, a wide range of relative orientations between helix H1 and the rest of the molecule. This potential ability to form arrays that conform to different curvatures could enable apo A-II to displace apo A-I from particles with a diverse distribution of sizes, to which antiparallel apo A-I dimers are expected to bind (*24*). Although only octamers are observed in A-II-BOG, the nature of the head-to-tail interaction does not preclude formation of larger oligomers.

Stability of Apo A-II−Lipid Interactions. Although no human HDL composed of only A-II have been observed, human apo A-II can completely displace apo A-I from canine HDL particles (*13*). Thermal and chaotrope-induced denaturation studies (*57*, *58*) also indicate that apo A-II forms more stable complexes with HDL. Both properties have been attributed to the stronger hydrophobicity of the apo A-II C-terminal helix to any in apo A-I (*26*). The A-II-BOG

structure, however, suggests that additional stability might be conferred on A-II−HDL complexes, containing multiple A-II dimers, by the polar interactions that we observe between dimers in head-to-tail oligomers. Observations on systems comparable to HDL have estimated the ΔG of association of two molecules of apo A-II with lipid to be −16.8 kcal compared to a value of −7.9 kcal/mol for apo A-I (*13*). A solvent accessible hydrogen bond contributes roughly 1 kcal/mol to stabilization (*59*); thus, the five head-to-tail interactions in each dimer of apo A-II in A-II-BOG could be responsible for more than one-quarter of the additional $\Delta\Delta G$ (−17.8 kcal/mol) in favor of apo A-II in a sequentially linked tetramer; an even larger contribution is expected if the charges are buried (*59*). Although main chain atoms of all pairs in the inner strand are almost totally buried, only those of the J−L tandem are approximately 50% buried in the outer octamer. Nevertheless, it is conceivable that many more might well be buried in the greater hydrophobic environment of an HDL particle. Furthermore, the head-to-tail association is mediated between primarily main chain atoms (carboxylates of the terminal residues of one chain with the amino nitrogen of the succeeding chain). This would make the property of association impervious to mutations of side chains and even to shortening of the chain, as long as it does not alter the positioning of the hydrophobic patches. For example, the last hydrophobic residue of the carboxyl-terminal hydrophobic patch is Leu70, with residues beyond this being in a coil conformation in most chains (Figure 3b). Thus, losing five or six residues from the carboxyl terminus, in the absence of destabilization of the adjoining helix, might not significantly impair the head-to-tail association of the protein.

Belt versus Picket-Fence Models. Two distinct configurations have been proposed for the relative orientation of lipid acyl chains in apo A-I binding to discoidal particles: the "picket-fence" model in which lipid acyl groups are parallel to local helical axes of the protein (*60*) and the "belt" model in which the protein wraps around the circumference of the disk, making acyl side chains parallel to local protein helical axes (*24*, *61*). Octyl chains of 58 of the 67 BOGs (87%) adopt a nearly perpendicular orientation (Figure 3b), with the inclination angle to the local apo A-II helix axis being between 75 and 115°. This observation, in conjunction with similarities in curvature between apo A-I and apo A-II (Figure 6a,b), appears to strongly favor the belt model for the disposition of apo A-II, and perhaps other apolipoproteins, in HDL.

The three structures we have presented together provide a structural basis for many experimental and computational results that have been obtained on apolipoproteins and their interactions with lipids. Amphipathic helices in apo A-II show significant conformational variation as a function of their environment; the observed variations, around a common helical architecture, provide parameters that can be incorporated into computational models of apolipoprotein−lipid interactions. The almost invariably orthogonal orientation of BOG octyl chains with respect to helical axes of apo A-II lends strong support to belt models of apo A-I−HDL interactions. Other observations, including the tenuous associations of apo A-II monomers in the dimer, the greater stability of apo A-II−lipid interactions, and other aspects of apolipoprotein−HDL interactions, are consistent with the apo A-II conformation and specific oligomerization in the structures. These structures provide the first set of experimental parameters, at both the residue and the molecular levels, for the structural and functional study of apolipoprotein−lipid interactions.

ACKNOWLEDGMENT

We are indebted to G. M. Anantharamaiah and Christie Brouillette for a preview of the manuscript and suggestions for improvement. We thank C. M. Ogata (NSLS/X4A) and John Chrzas (APS/IMCA) for help with data measurement.

REFERENCES

1. Despres, J. P., Lemieux, I., Dagenais, G. R., Cantin, B., and Lamarche, B. (2000) *Atherosclerosis 153*, 263−272.
2. Stein, O., and Stein, Y. (1999) *Atherosclerosis 144*, 285−301.
3. Hajjar, K. A., and Nachman, R. I. (1996) *Annu. Rev. Med. 47*, 423−442.
4. Plutzky, J. (2000) *Curr. Opin. Cardiol. 15*, 416−421.
5. Yokoyama, S. (1998) *Biochim. Biophys. Acta 1392*, 1−15.
6. Eckerdstein, A. v., Nofer, J.-R., and Assman, G. (2001) *Arterioscler. Thromb. Vasc. Biol. 21*, 13−27.
7. Small, D. M. (1987) *Atheroscler. Rev. 16*, 1−9.
8. Rothblat, G. H., Llera-Moya, M. d. l., Atger, V., Kellner-Weibel, G., Williams, D. L., and Phillips, M. C. (1999) *J. Lipid Res. 40*, 781−796.
9. Blanco-Vaca, F., Escola-Gil, J. C., Martin-Campos, J. M., and Julve, J. (2001) *J. Lipid Res. 42*, 1727−1739.
10. Castellini, L. W., and Lusis, A. J. (2001) *Arterioscler. Thromb. Vasc. Biol. 21*, 1870−1872.
11. Holvoet, P., Peeters, K., Lund-Katz, S., Mertens, A., Verhamme, P., Quarck, R., Stengel, D., Lox, M., Deridder, E., Bernar, H., Theilmeier, G., Ninio, E., and Phillips, M. C. (2001) *Arterioscler. Thromb. Vasc. Biol. 21*, 1977−1983.
12. Durbin, D. M., and Jonas, A. (1999) *J. Lipi. Res. 40*, 2293−2302.
13. Logocki, P., and Scanu, A. M. (1980) *J. Biol. Chem. 255*, 3701−3706.
14. Edelstein, C., Halari, M., and Scanu, A. M. (1982) *J. Biol. Chem. 257*, 7189−7195.
15. Kwiterovich, P. O., Jr. (2000) *Am. J. Cardiol. 86*, 5L−10L.
16. Jonas, A. (1992) in *Structure and Function of Apolipoproteins* (Rosseneu, M., Ed.) pp 138−152, CRC Press, Boca Raton, FL.
17. Brooks-Wilson, A., Marcil, M., Clee, S. M., Zhang, L. H., Roomp, K., van Dam, M., Yu, L., Brewer, C., Collins, J. A., Molhuizen, H. O., Loubser, O., Ouelette, B. F., Fichter, K., Ashbourne-Excoffon, K. J., Sensen, C. W., Scherer, S., Mott, S., Denis, M., Martindale, D., Frohlich, J., Morgan, K., Koop, B., Pimstone, S., Kastelein, J. J., and Hayden, M. R. (1999) *Nat. Genet. 22*, 336−345.
18. Bodzioch, M., Orso, E., Klucken, J., Langmann, T., Bottcher, A., Diederich, W., Drobnik, W., Barlage, S., Buchler, C., Porsch-Ozcurumez, M., Kaminski, W. E., Hahmann, H. W., Oette, K., Rothe, G., Aslanidis, C., Lackner, K. J., and Schmitz, G. (1999) *Nat. Genet. 22*, 347−351.
19. Rust, S., Rosier, M., Funke, H., Real, J., Amoura, Z., Piette, J. C., Deleuze, J. F., Brewer, H. B., Duverger, N., Denefle, P., and Assmann, G. (1999) *Nat. Genet. 22*, 352−355.
20. Ji, Y., Jian, B., Wang, N., Sun, Y., Moya, M. d. l. L., Phillips, M. C., Rothblat, G. H., Swaney, J. B., and Alan, R. T. (1997) *J. Biol. Chem. 272*, 20982−20985.
21. Krieger, M. (1999) *Annu. Rev. Biochem. 68*, 523−558.
22. Fisher, C. A., and Ryan, R. O. (1999) *J. Lipid Res. 40*, 93−99.
23. Frank, P. G., and Marcel, Y. L. (2000) *J. Lipid Res. 41*, 853−872.
24. Borhani, D. W., Rogers, D. P., Engler, J. A., and Brouillette, C. G. (1997) *Proc. Natl. Acad. Sci. U.S.A. 94*, 12291−12296.
25. Frank, P. G., N'Guyen, D., Franklin, V., Neville, T., Desforges, M., Rassart, E., Sparks, D. L., and Marcel, Y. L. (1998) *Biochemistry 37*, 13902−13909.
26. Segrest, J., Jones, M., De Loof, H., Brouillette, C., Venkatachalapathi, Y., and Anantharamaiah, C. (1992) *J. Lipid Res. 33*, 141−166.
27. Brouillette, C. G., Anamtharamaiah, G. M., Engler, J. A., and Borhani, D. W. (2001) *Biochim. Biophys. Acta 1531*, 4−46.

28. Narayanaswamy, V., and Ryan, R. O. (2000) *Biochim. Biophys. Acta 1483*, 15−36.
29. Brouillette, C. G., and Anantharamaiah, G. M. (1995) *Biochim. Biophys. Acta 1256*, 103−109.
30. Breiter, D. R., Kanost, M. R., Benning, M. M., Wesenberg, G., Law, J. H., Wells, M. A., Rayment, I., and Holden, H. M. (1991) *Biochemistry 30*, 603−608.
31. Wilson, C., Wardell, M. R., Weisgraber, K. H., Mahley, R. W., and Agard, D. A. (1991) *Science 252*, 1817−1822.
32. Wang, J., Sykes, B. D., and Ryan, R. O. (2002) *Proc. Natl. Acad. Sci. U.S.A. 99*, 1188−1193.
33. MacRaild, C. D., Hatters, D. M., Howlett, G. J., and Gooley, P. R. (2001) *Biochemistry 40*, 5414−5421.
34. Garavito, R. M. (1991) in *Crystallization of Membrane Proteins* (Michel, H., Ed.) pp 89−106, CRC Press, Boca Raton, FL.
35. Weiswaler, P. (1987) *Clin. Chim. Acta 169*, 249−254.
36. Kabsch, W. (1988) *J. Appl. Crystallogr. 21*, 916−924.
37. Terwilliger, T. C., and Berendzen, J. (1999) *Acta Crystallogr. D55*, 849−861.
38. Otwinowski, Z. (1991) in *Daresbury Study Weekend Proceedings* (Wolf, W., Evans, P. R., and Leslie, A. G. W., Eds.) pp 101−107, Daresbury Laboratory, Warrington, U.K.
39. Cowtan, K. (1994) in *Joint CCP4 and ESF-EACBM Newsletter on Protein Crystallography* (Bailey, S., Ed.) pp 34−38, Daresbury Laboratory, Warrington, U.K.
40. Jones, T. A., Zou, J. Y., Cowans, S. W., and Kjeldgaard, M. (1991) *Acta Crystallogr. A47*, 110−119.
41. Brunger, A. T., Adams, P. D., Clore, G. M., DeLano, W. L., Gros, P., Grosse-Kunstleve, R. W., Jiang, J.-S., Kuszewski, J., Nilges, M., Pannu, N. S., Read, R. J., Rice, L. M., Simonson, T., and Warren, G. L. (1998) *Acta Crystallogr. D54*, 905−921.
42. Engh, R. A., and Huber, R. (1991) *Acta Crystallogr. A47*, 392−400.
43. Carson, M. C. (1996) *J. Comput.-Aided Mol. Des. 10*, 273−283.
44. Sheldahl, C., and Harvey, S. C. (1999) *Biophys. J. 76*, 1190−1198.
45. Connolly, M. L. (1993) *J. Mol. Graphics 12*, 139−141.
46. Collaborative Computational Project No. 4 (1993) *Acta Crystallogr. D55*, 760−763.
47. Gordon, J. I., Budelier, K. A., Sims, H. F., Edelstein, C., Scanu, A. M., and Strauss, A. W. (1983) *J. Biol. Chem. 258*, 14054−14059.
48. Hussain, M. M., and Zannis, V. I. (1990) *Biochemistry 29*, 209−217.
49. Hutchinson, E. G., and Thornton, J. M. (1996) *Protein Sci. 5*, 212−220.
50. De Coen, J.-L., Deboeck, M., Delcroix, C., Lontie, J.-F., and Malmendier, C. L. (1988) *Proc. Natl. Acad. Sci. U.S.A. 85*, 5669−5672.
51. Tsai, C.-J., Lin, S. L., Wolfson, H. J., and Nussinov, R. (1997) *Protein Sci. 6*, 53−64.
52. Gursky, O., and Atkinson, D. (1996) *Protein Sci. 5*, 1874−1882.
53. Anantharamaiah, G. M. (1986) in *Methods in Enzymology* (Colowick, S. P., and Kaplan, N. O., Eds.) pp 627−646, Academic Press, New York.
54. Diamond, R. (1992) *Protein Sci. 1*, 1279−1287.
55. Saito, H., Dhanasekaran, P., Baldwin, F., Weisgraber, K. H., Lund-Katz, S., and Phillips, M. C. (2001) *J. Biol. Chem. 276*, 40949−40954.
56. Segrest, J. P., Jones, M. K., Klon, A. E., Sheldahl, C. J., Hellinger, M., Loof, H. D., and Harvey, S. C. (1999) *J. Biol. Chem. 274*, 31655−31758.
57. Tall, A. R., Deckelbaum, R. J., Small, D. M., and Shipley, G. G. (1977) *Biochim. Biophys. Acta 487*, 145−153.
58. Nichols, A. V., Gong, E. L., Forte, T. M., and Anderson, D. W. (1976) *Biochim. Biophys. Acta 446*, 226−239.
59. Dill, K. A. (1990) *Biochemistry 29*, 7133−7155.
60. Nolte, R. T., and Atkinson, D. (1992) *Biophys. J. 63*, 1221−1239.
61. Koppaka, V., Silvestro, L., Engler, J. A., Brouillette, C. G., and Axelsen, P. H. (1999) *J. Biol. Chem. 274*, 14541−14544.

BI026069W